Biological
Cybernetics

Measuring information transfer in the spike generator of crayfish sustaining fibers

Methods and analysis

Christopher J. Rozell[1], Don H. Johnson[1], Raymon M. Glantz[2]

[1] Department of Electrical & Computer Engineering, Rice University, Houston, TX, 77251
[2] Department of Biochemistry & Cell Biology, Rice University, Houston, TX, 77251

Abstract. We present a method based on information-theoretic distances for measuring the information transfer efficiency of voltage to impulse encoders. In response to light pulses, we simultaneously recorded the EPSP and spiking output of crayfish sustaining fibers. To measure the distance between analog EPSP responses, we developed a membrane noise model that accurately captures stimulus-induced nonstationarities. By comparing the EPSP and spike responses, we found encoding efficiencies on the order of 10^{-4}, with interesting dynamics occurring during initial transients. A simple analog to point-process converter predicted the small information transfer efficiencies and dynamic properties we measured.

1 Introduction and background

Most sensory systems convert an essentially analog representation of an external stimulus into a spike train representation that is used in higher-level processing. A step toward understanding the processing performed in sensorineural systems is quantifying the information efficiency of the voltage to impulse encoder performing this conversion. In this work we present methods for measuring the information transfer efficiency of a voltage to impulse encoding mechanism and illustrate these methods by analyzing a unit from the early visual pathway of the crayfish.

1.1 Data collection in the crayfish visual pathway

The retina of the crayfish compound eye has groups of photoreceptors organized in ommatidia. The receptor axons project to lamina ganglion cells, and these project in columnar fashion to interneurons in the medulla externa. These retinotopically organized interneurons synapse on sustaining fiber (SF) dendrites. The 14 distinct SFs have input EPSPs closely resembling graded and delayed versions of summed photoreceptor activity over a segment of the visual field (Kirk et al. 1983; Waldrop and Glantz 1985). The SFs are most likely the first stage where an analog (EPSP) signal representing an external visual stimulus is converted into a spike train. Thus, the SFs represent a "front end" for information processing in higher centers of the brain. This is illustrated schematically in Figs. 1 and 2.

Both SF input EPSPs and output spike trains exhibit transient and steady-state behavior proportional to stimulus intensity (Kirk et al. 1982; Wiersma and Yamaguchi 1966). To examine the information transfer efficiency of the SF voltage to impulse encoder during the transient and steady-state response segments, dark-adapted crayfish are repeatedly presented with a sudden-onset stimulus having intensity values chosen from a predetermined set. The strong spike responses generated in the SF are involved in controlling an eyestalk reflex (Miller et al. 2002, 2003). The stimuli therefore induce an information-bearing response in the SF that is biologically relevant. Intracellular SF recordings are made during stimulus presentation with a microelectrode placed near the spike-initiating zone. The SF is tested with a range of stimulus values, and data collection begins when we ascertain that the responses are adapted to the stimulus. Data collection experimental methods are described in Kirk et al. (1982, 1983) and Waldrop and Glantz (1985). The intracellular recordings are a composite of the EPSP and the resulting spike train, which are separated using a method based on wavelet denoising (Rozell 2002).

1.2 A theory of information processing

We would like to understand the transmission of stimulus information from the EPSP to the impulse

---

Correspondence to: C. J. Rozell
(e-mail: crozell@rice.edu, Fax: +1-713-3485686)
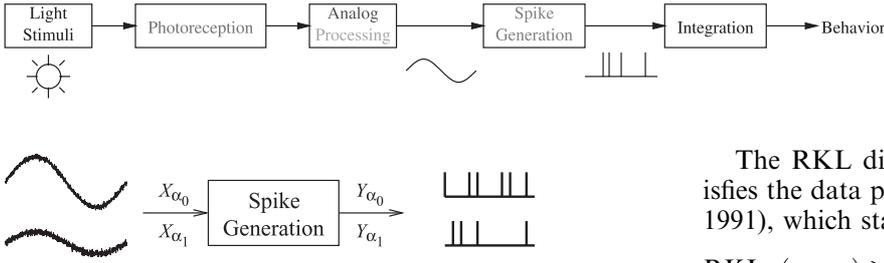
Fig. 2. The SF voltage to impulse encoder has an analog EPSP input (X_α) and a spike train output (Y_α) that both depend on the value of the input stimulus (α)

train. Many standard signal processing techniques cannot be applied to this problem because of the disparity between the analog input and the spike train output. However, a recent theory quantifies a system's information processing capabilities regardless of the form of its input and output signals (Johnson et al. 2000, 2001; Sinanović and Johnson 2004, manuscript in preparation). This information processing theory is the basis of the current analysis, and we summarize it here.

Information (such as a stimulus light intensity parameter) is conveyed by a stochastic signal with a probability law that depends on the exact information value. Stimulus parameters are expressed by the vector $\boldsymbol{\alpha}$, and the stochastic analog EPSP representing that stimulus is given by X_α. Here X_α is distributed according to p_α, a probability function that depends on $\boldsymbol{\alpha}$. The SF voltage to impulse encoder takes X_α as input and produces the stochastic spike train Y_α (governed by a probability law q_α) as output. We would like to compare the amount of information about $\boldsymbol{\alpha}$ that can be extracted from the input and output signals. We quantify the amount of information a signal contains with regard to a specific stimulus feature by inducing controlled *changes* in the value of $\boldsymbol{\alpha}$ and measuring the *changes* in X_α and Y_α (reflecting the differing information content). Given two different values of stimulus parameter $\boldsymbol{\alpha}$, we compute the Kullback-Leibler (KL) distance (Cover and Thomas 1991) between the probability distributions describing the EPSPs under $\boldsymbol{\alpha}_0$ and $\boldsymbol{\alpha}_1$,

$$\mathrm{KL}_X(\boldsymbol{\alpha}_1, \boldsymbol{\alpha}_0) = \int p_{\boldsymbol{\alpha}_1}(\boldsymbol{x}) \log_2 \frac{p_{\boldsymbol{\alpha}_1}(\boldsymbol{x})}{p_{\boldsymbol{\alpha}_0}(\boldsymbol{x})} \mathrm{d}\boldsymbol{x} \quad, \tag{1}$$

having units of "bits". The KL distance is generally asymmetric, which presents problems in an experimental setting.[1] A symmetrized extension called the *resistor-averaged KL* (RKL),

$$\mathrm{RKL}_X(\boldsymbol{\alpha}_1, \boldsymbol{\alpha}_0) = \frac{\mathrm{KL}_X(\boldsymbol{\alpha}_0, \boldsymbol{\alpha}_1)\mathrm{KL}_X(\boldsymbol{\alpha}_1, \boldsymbol{\alpha}_0)}{\mathrm{KL}_X(\boldsymbol{\alpha}_0, \boldsymbol{\alpha}_1) + \mathrm{KL}_X(\boldsymbol{\alpha}_1, \boldsymbol{\alpha}_0)} \quad, \tag{2}$$

is computed at both the SF's input and output. The KL distance can be related to the performance of both optimal detectors and estimators (Johnson et al. 2001).

The RKL distance (as well as the KL distance) satisfies the data processing inequality (Cover and Thomas 1991), which states that

$$\mathrm{RKL}_X(\boldsymbol{\alpha}_1, \boldsymbol{\alpha}_0) \geq \mathrm{RKL}_Y(\boldsymbol{\alpha}_1, \boldsymbol{\alpha}_0) \quad. \tag{3}$$

In other words, while systems can convert a signal from one form to another, no amount of processing can increase the signal's fidelity in representing $\boldsymbol{\alpha}$. Given a change in stimulus parameter $\boldsymbol{\alpha}$, the ratio of the distance at the output to the distance at the input,

$$\gamma_{X,Y}(\boldsymbol{\alpha}_0, \boldsymbol{\alpha}_1) = \frac{\mathrm{RKL}_Y(\boldsymbol{\alpha}_0, \boldsymbol{\alpha}_1)}{\mathrm{RKL}_X(\boldsymbol{\alpha}_0, \boldsymbol{\alpha}_1)} \quad, \tag{4}$$

quantifies the amount of information about $\boldsymbol{\alpha}$ that was suppressed by the system. From the data processing inequality (3) it follows that $0 \leq \gamma_{X,Y} \leq 1$, where a value of 1 represents perfect information transfer of the change in $\boldsymbol{\alpha}$ from input to output, and a value of zero means all information about $\boldsymbol{\alpha}$ was suppressed.

An information processing analysis (based on KL distances) is fundamentally different from an analysis using mutual information or capacity (Cover and Thomas 1991). KL distances are directly related to the (asymptotic) exponential error decay rate of optimal detectors and the performance of optimal mean-squared error estimators operating on the input and output signals. The KL distance is very general, and a KL-based analysis does not assume linearity or Gaussianity. However, in the Gaussian case the KL distance corresponds exactly to the Fisher discriminant. The ratio of KL distances can be directly related to the relative performance loss of optimal systems processing the input and output signals. In contrast, mutual information is a measure of statistical dependence and has no direct relation to extracting information from signals. Mutual information and capacity have completely different interpretations in the framework of digital communications (Shannon and Weaver 1949) or rate-distortion theory (Berger 1971). Examples show that the ratio of KL distances ($\gamma_{X,Y}$) can be arbitrarily different from mutual information, and thus they are not related in general. A complete description of this information processing theory can be found in Sinanović and Johnson (2004, manuscript in preparation).

2 Estimating RKL distances

SFs have spike train outputs, and an information processing analysis requires RKL distance calculations between spike train probability laws under two different stimulus conditions. Johnson et al. (2001) presented a method for estimating RKL distances using spike responses. To summarize, spike responses to a periodically repeated stimulus are binned (10-ms bins assure

---

[1] Note that the common terminology "KL distance" does not imply that it is a metric.

that most SF bins have only one event), and the probability of events occurring in each bin is estimated for both stimulus conditions. If the bins are independent, the total RKL distance between the responses is the sum of the RKL distances calculated for each individual bin. A Markov dependence structure between bins can be included but requires exponentially more data. The datasets available are not large enough for reliable estimates when including Markov dependence, so we assume independent bins. This quantity approximates, but does not bound, the true distance (including interbin dependencies). We have verified that the independent bin assumption introduces insignificant error by calculating spike RKL distances assuming first-order Markov dependence on both larger SF datasets and simulated data with the same first-order statistics as the SF spike responses. In the worst case (using the simulated data), we observe an increase of a factor of two in the estimated RKL when including interbin dependence. This error will prove to be insignificant given the order of magnitude of our measurements. Spike response RKL distance estimates can be considerably biased. The bootstrap (Hall 1992), a statistical resampling technique, has been used successfully to remove bias and calculate confidence intervals in spike response RKL estimates (Gruner 1998; Johnson et al. 2001).

We also need to estimate the RKL distance between probability laws governing the analog EPSP inputs. The compound EPSP input signal (measured near the integration region of the SF) is a sum of many individual EPSP events initiated in the dendritic tree. These individual events are the direct result of neurotransmitter release in the synapse, which is a quantal process. The quantal events have a sudden onset with a relatively quick decay, and the sum can be conceptualized as "shot noise" (Papoulis 1965). Asymptotically, the sum of many such individual EPSP "shots" is a Gaussian random process. We verified the marginal normality by applying a Kolmogorov-Smirnov-type goodness-of-fit test (Conover 1980) to a segment of recorded data from the resting SF membrane.[2] Data samples passed with a significance level of at least 0.01.

Using Gaussian random vector assumptions for sampled EPSPs under two stimulus conditions, $X_{\boldsymbol{\alpha}_0} \sim N(\boldsymbol{\mu}_{\boldsymbol{\alpha}_0}, \mathbf{K})$ and $X_{\boldsymbol{\alpha}_1} \sim N(\boldsymbol{\mu}_{\boldsymbol{\alpha}_1}, \mathbf{K})$, the RKL is

$$\text{RKL}_X(\boldsymbol{\alpha}_0, \boldsymbol{\alpha}_1) = \frac{(\boldsymbol{\mu}_{\boldsymbol{\alpha}_1} - \boldsymbol{\mu}_{\boldsymbol{\alpha}_0})^t \mathbf{K}^{-1} (\boldsymbol{\mu}_{\boldsymbol{\alpha}_1} - \boldsymbol{\mu}_{\boldsymbol{\alpha}_0})}{4} \quad . \qquad (5)$$

The mean vectors ($\boldsymbol{\mu}_{\boldsymbol{\alpha}_0}$ and $\boldsymbol{\mu}_{\boldsymbol{\alpha}_1}$) and covariance matrix ($\mathbf{K}$) are needed to estimate the input distance. We estimate the mean vector $\boldsymbol{\mu}_{\boldsymbol{\alpha}}$ for each stimulus condition by averaging EPSP responses. Estimating $\mathbf{K}$ (the correlation structure of the membrane noise) presents significant difficulties, particularly because the membrane typically has time-varying characteristics. Direct estima-

tion of the sample covariance matrix is not desirable because the datasets are small compared to the size of $\mathbf{K}$. To estimate the distance between two EPSP responses, we examine a membrane noise correlation model based on membrane physiology.

2.1 Membrane noise correlation

The primary neural structures contributing to EPSP formation are functionally analogous to electrical components, leading naturally to neurophysiologic circuit models. The resting membrane has a characteristic conductance (G_{mem}), and an EPSP occurs when post-synaptic ligand-gated ion channels open, increasing the synaptic conductance $\left(G_{syn}(t)\right)$. The net membrane conductance is the sum of the synaptic and resting membrane conductances, $G(t) = G_{syn}(t) + G_{mem}$. The ion channel ensembles are modeled as a membrane resistor and a synaptic variable resistor in parallel with a membrane capacitor. The circuit model for the membrane is the first-order RC lowpass filter shown in Fig. 3. Conductance increases responsible for EPSP generation have been measured in crayfish SFs by Waldrop and Glantz (1985). Resting membrane conductances and membrane capacitances for the SF units can be derived from the RC model, the results of Waldrop and Glantz (1985), and the empirically measured membrane time constant (15–25 ms). The active membrane acts as a lowpass filter with a *time-varying* pole at $-G(t)/C_{mem}$ (Siebert 1986). RC circuit models and the underlying neural processes are continuous-time systems. However, during data collection the true membrane activity is sampled and all data processing must be done in discrete time. We use the *impulse invariance* method (Oppenheim et al. 1999) to convert the RC circuit model in Fig. 3 to an approximately equivalent single-pole, discrete-time filter.

A sampled version of the time-varying conductance $G(n)$ is determined according to the relationship measured in Waldrop and Glantz (1985) using the EPSP value at time step n and the membrane resting conductance. Using the impulse invariance method, the time-varying, discrete-time pole locations $a(n)$ are given according to the equation $a(n) = \exp\{-G(n)/(C_{mem}F_s)\}$, where F_s is the sampling frequency (10^3 Hz in our case) (Rozell 2002). An example EPSP is shown in Fig. 4, along with the time-varying net membrane resistance $R(n) = 1/G(n)$ and the corresponding pole location $a(n)$.
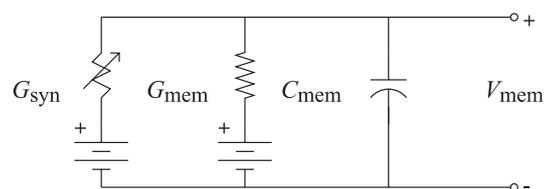
Fig. 3. The neural membrane is modeled as a first-order RC circuit, where V_{mem} is the membrane voltage, G_{mem} the resting membrane conductance, G_{syn} the variable synaptic conductance, and C_{mem} the membrane capacitance

---

[2]The resting membrane has no significant EPSP signal present, and the corresponding static synaptic conductance provides the most stationary data sample we can observe.
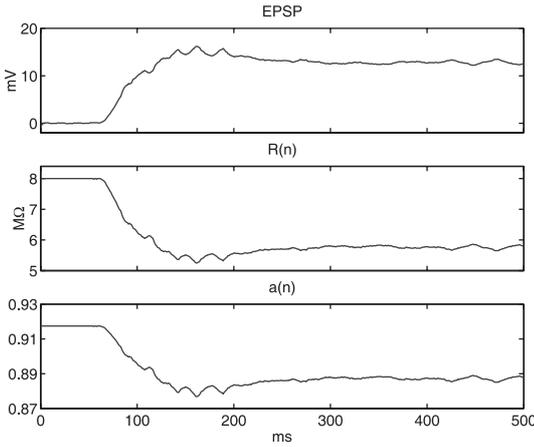
Fig. 4. Shown in the *top panel* is an example SF EPSP deflection from a sudden onset stimulus. In this example, the resting membrane has a conductance of $G_{mem} = 1/8\,\mathrm{M\Omega}$ and a capacitance of $C = 1.45\,\mathrm{nF}$. The time-varying resistance $R(n) = 1/G(n)$ generating the EPSP is shown in the *middle panel*. The resulting time-varying pole location $a(n)$ of the equivalent discrete-time system is shown in the *bottom panel*

The nonstationary, discrete-time system is described by the difference equation

$$y(n) = a(n)y(n-1) + x(n) \ . \tag{6}$$

The discrete-time system in (6) has a unit-sample response given by

$$h(n,k) = \left(\prod_{l=k+1}^{n} a(l) u(n-k) \right) + \delta(n-k) \ , \tag{7}$$

where $u(n)$ is the unit-step function and $h(n,k)^3$ is the response of the system at time step n to $\delta(n-k)$, a unit sample at time step k. The nonstationary system described by (7) is the basis for a SF membrane noise model used in estimating EPSP RKL distances. Artificial membrane noise generated using the present model appears to contain the dominant spectral characteristics observed in the EPSP data.

2.2 Model-based EPSP RKL calculation

The unit sample response given in (7) can be used to calculate the term in the n-th row and m-th column of the membrane noise covariance matrix,

$$\mathbf{K}(n,m) = \sigma^2 \left(1 - a_0^2 \right)$$

$$\times \left[\delta(m-n) + \left(\prod_{k=m+1}^{n} a(k) \right) + \left(\prod_{r=n+1}^{m} a(r) \right) \right. $$

$$\left. + \sum_{l=1}^{\infty} \left(\prod_{k=n-l+1}^{n} a(k) \prod_{r=n-l+1}^{m} a(r) \right) \right] , \tag{8}$$

---

[3] It is important to note a notation convention. The product operator is defined to be zero for any terms where the lower index exceeds the upper index, $\prod_{l=\alpha}^{\beta} x(l) = 0, \alpha > \beta$.

where σ^2 and a_0 are estimates of the colored noise variance and pole location of the resting membrane. More details on (8) are given in Appendix 4, and a complete derivation can be found in Rozell (2002).

The membrane noise model leads to a simple algorithm for calculating EPSP RKL distances. Under each stimulus condition, we averaged the EPSP responses to find the mean signal $\boldsymbol{\mu}_\alpha$. The resting membrane conductance G_{mem} determines the resting membrane pole location, a_0. We used a resting segment of the EPSP recording to estimate the noise variance, σ^2. During active membrane periods, we used the mean EPSP deflection signal to calculate the values of $G(n)$ according to the relationship measured in Waldrop and Glantz (1985) and using the membrane resting conductance (G_{mem}). The membrane capacitance C_{mem} and the time-varying membrane conductance $G(n)$ are used to find the time-varying pole location $a(n)$ using the impulse invariance method. Having $a(n)$, a_0, σ^2, and the correlation function $\mathbf{K}(n,m)$ in (8), we formed an estimate of the covariance matrix $\mathbf{K}$. Using mean EPSP signals $(\boldsymbol{\mu}_{\alpha_0}, \boldsymbol{\mu}_{\alpha_1})$ and covariance matrix $\mathbf{K}$, we estimate the RKL distance between input responses according to (5).

3 Data analysis

We applied the EPSP and spike train RKL estimation methods described in Sect. 2 to data collected from crayfish SFs. The ratio of RKL estimates are calculated for SFs responding to a range of stimulus values. The dataset consists of responses to sudden-onset stimuli with log intensity values chosen from the set $LI_1 = \{-3.5, -3.0, -2.5, -2.0, -1.5, -1.0\}$, ordered from weakest to strongest. A single trial consists of a dark adapting period followed by a suddenly applied static stimulus covering the SF receptive field. In this preparation, the membrane capacitance and resting conductance were determined to be 1.45 nF and $1/(8.0\,\mathrm{M\Omega})$, respectively. Mean EPSP deflection signals elicited from the stimuli are shown in Fig. 5. The EPSPs exhibit quick positive deflections at stimulus onset, with magnitude and slope increasing with stimulus intensity. The transient lasts approximately 150 ms, followed by a decay to a steady state. The spike response poststimulus time (PST) histograms elicited from the stimuli are shown in Fig. 6. The spike responses also exhibit transient and steady-state behavior with an initial burst of spikes followed by a drop to relatively constant rates.

Cumulative RKLs are estimated using input and output responses for all possible pairs of stimuli conditions in the dataset. Figure 7 shows the cumulative input EPSP RKL distances for all possible pairs of stimuli. A few general trends are worth noting. As expected, stimuli pairs farther apart in intensity (signified by plots more toward the lower left corner of Fig. 7) tend to produce responses that have a larger total EPSP RKL distance than pairs closer together. Cumulative EPSP RKLs also generally show two distinct time segments: a large RKL accumulation rate during the transient response and a smaller RKL accumulation rate over the steady-state
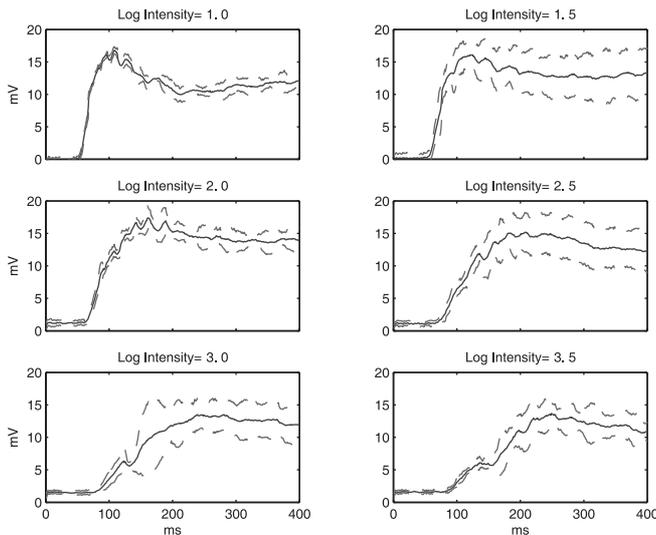
Fig. 5. Mean EPSP deflections in a SF responding to sudden-onset stimuli of different log intensities (with 90% confidence intervals)
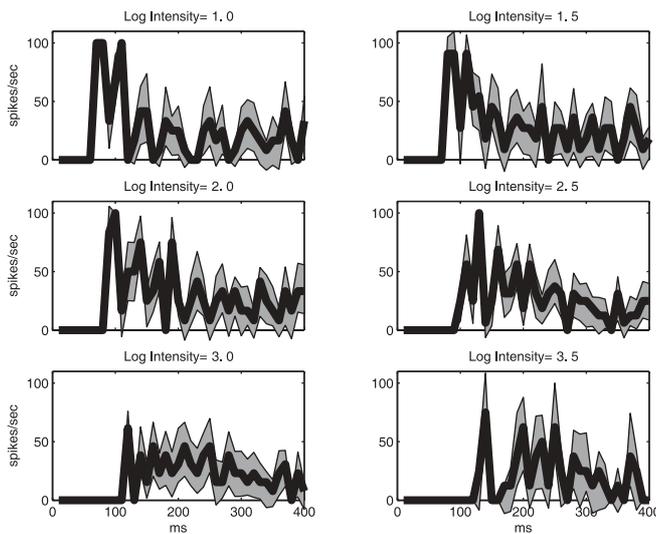
Fig. 6. Poststimulus time (PST) histograms for the SF responding to sudden-onset stimuli of different log intensities (with 90% confidence intervals generated using the bootstrap procedure, Hall 1992)

response. The difference in RKL accumulation rates is observed in the large slope of the cumulative RKL plot during the first 100 ms, followed by a much smaller slope during the remaining response. For example, the stimulus pair $\{\alpha_0 = -1.0, \alpha_1 = -3.5\}$ shows a large EPSP RKL accumulation rate of roughly 5×10^5 bits/s during the transient response and 4×10^4 bits/s during the remaining response. The EPSP RKL accumulation rates are more than an order of magnitude different during the transient and steady-state time segments in this example.

Similarly, output (spike train) cumulative RKL distances for all possible stimuli pairs are shown in Fig. 8. Cumulative spike RKLs tend to show roughly the same transient and steady-state behavior as cumulative EPSP RKLs. The difference immediately evident is the scale:

the spike RKLs are four orders of magnitude smaller than the EPSP RKLs. The $\{\alpha_0 = -1.0, \alpha_1 = -3.5\}$ stimulus pair shows spike RKL accumulation rates of roughly 50 bits/s during the transient response and 4 bits/s during the remaining response. Again, the difference between transient and steady-state spike RKL accumulation rates is roughly one order of magnitude. However, the spike RKL accumulation rates are four orders of magnitude smaller than the EPSP RKL accumulation rates.

The time-varying ratio of spike train and EPSP cumulative RKLs ($\gamma_{X,Y}$) for all possible stimuli pairs are shown in Fig. 9. Error bars are plotted using the EPSP RKL estimates and spike RKL estimate error bars. We cannot directly calculate error bars for the EPSP RKL estimates (and consequently for the information transfer ratio estimates) because of the estimator complexity. Therefore, the error bars shown are a lower limit for the true error bar width. The most significant time-varying trend in $\gamma_{X,Y}$ is the tendency to peak sharply during the transient SF response and decay to a relatively constant value. These peaks appear more pronounced for *small* changes in the stimulus value, and the peaks can be nearly an order of magnitude greater than the steady-state values. The steady-state ratio of RKLs values are relatively invariant to the size of the stimulus change, always yielding a final value in the range $(0.6\text{--}2) \times 10^{-4}$.

3.1 Theoretical analog to point-process converter

The preceding analysis illuminated some general trends: very low values of $\gamma_{X,Y}$ and time-varying information processing capabilities. In SF spike responses, the initial transient rates cannot be explained by a simple scaling of the EPSPs. Sudden EPSP *changes* also play a role in increasing the discharge rate. To explore the role of ideal systems converting analog signals into point processes, we use a simple time-varying model that takes a Gaussian random process $\widetilde{X}(t)$ and produces a Poisson process $\widetilde{Y}(t)$ with intensity function

$$\lambda(t) = A\widetilde{X}(t) + B\frac{\mathrm{d}\widetilde{X}(t)}{\mathrm{d}t} \quad . \tag{9}$$

The relationship in (9) has the same form as the equation for the current through an RC model of the membrane ($I(t) = GX(t) + C\frac{\mathrm{d}X(t)}{\mathrm{d}t}$), with A and B as steady-state and transient scaling constants. Equation (9) is not meant to model spike generation in any biological system but is simply an ideal analog to point-process converter (i.e., lossless except for the inherent noise in the point process).

The probability of event counts in a time bin $0 \leq t \leq T$ depends on the integral of the intensity function over that bin, $\Lambda(0, T) = \int_0^T \lambda(t)dt$. Because $\widetilde{X}(t)$ is a Gaussian random process, $\Lambda(0, T)$ is a Gaussian random variable. Given input random processes, the probability mass functions for event counts in the bin $0 \leq t \leq T$ and the resulting output RKL distance can be computed. A complete derivation of the density of $\widetilde{Y}(t)$ can be found
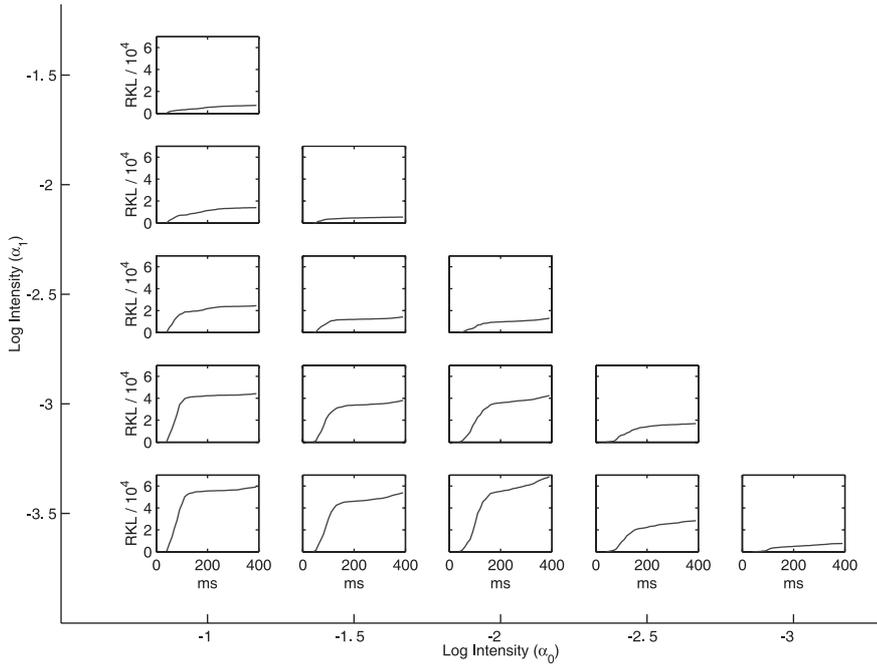
Fig. 7. SF input (EPSP) cumulative RKL distances for all stimuli pairs. The *outer axes* denote the log intensity values of the stimuli that elicited the responses (α_0 and α_1). The *inner axes* show the cumulative EPSP RKL distance for a particular stimuli pair. The y-axis of the inner plots is $RKL/10^4$ (units of bits)
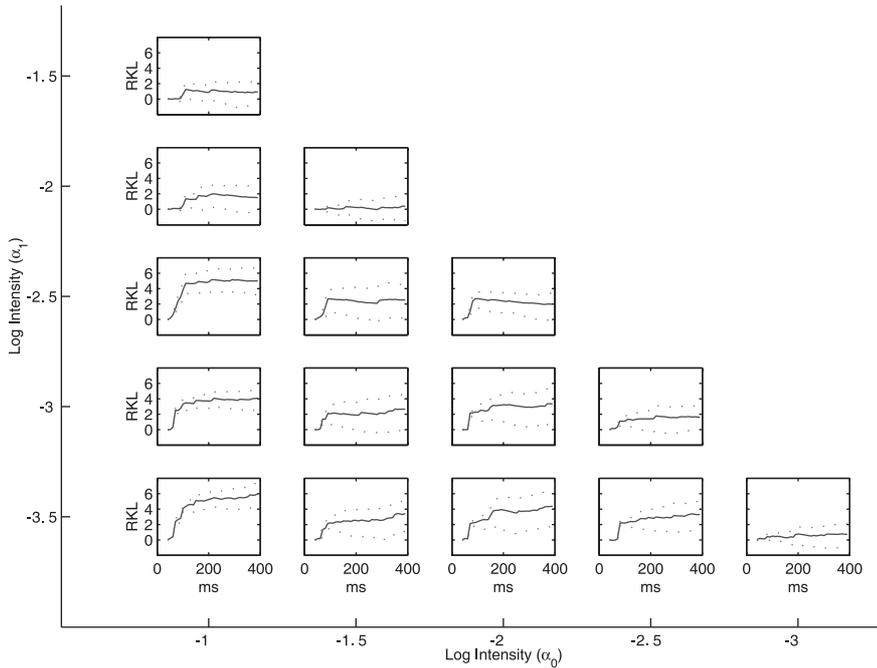
Fig. 8. SF output (spike) cumulative RKL distances for all stimuli pairs. The *outer axes* denote the log intensity values of the stimuli that elicited the responses (α_0 and α_1). The *inner axes* show the cumulative spike RKL distance for a particular stimuli pair. The y-axis of the *inner plots* is resistor-averaged RKL distance (units of bits). Error bars (90th percentile) estimated using the bootstrap procedure are shown as *dotted lines*

in (Rozell 2002). Using a sample pair of SF responses, we selected values of A and B that roughly predict SF discharge rates. Though (9) is not meant to model SF spike generation, it allows an exploration of a simple system with input signal-to-noise ratios and output event rates in the same range as the SF. The information processing characteristics of the system in (9) are shown in Fig. 10. The transient peak seen in the SF analysis is also present with our simple analog to point-process converter. Even though both input and output RKLs exhibit transient and steady-state behavior, it is not necessary that systems with time-varying behavior will automatically exhibit time-varying information

processing capabilities. To illustrate, the same theoretical analysis was repeated setting $B = 0$. The resulting input and output cumulative RKLs still show transient and steady-state behavior, though less pronounced in the output RKL. The time-varying ratio of RKLs is more constant and does not show a large obvious peak followed by a decay to a steady-state value.

4 Conclusions

The SF information processing characteristics are surprising because of their very low values. In this analysis,
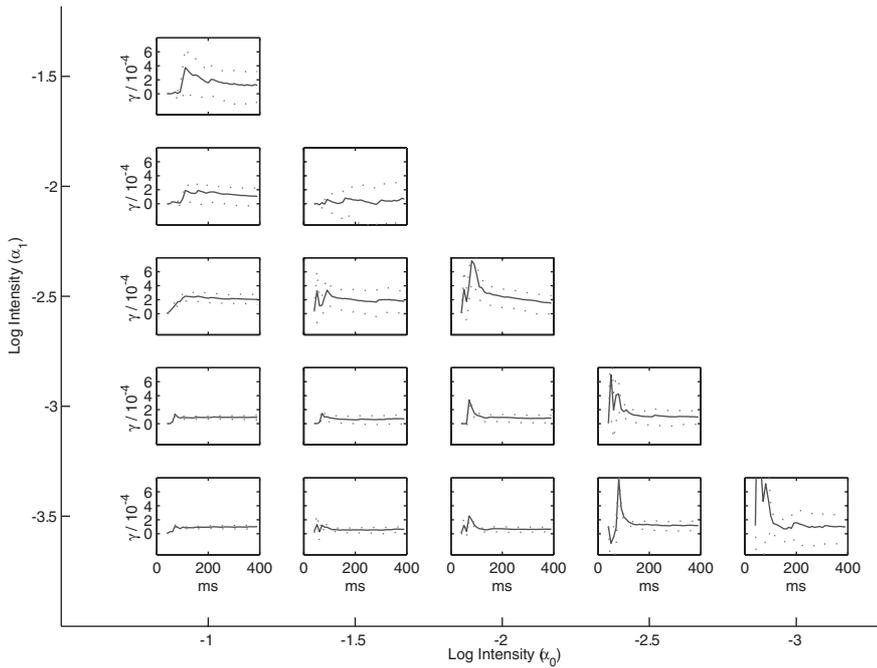
Fig. 9. SF time-varying ratios of RKL distances ($\gamma_{X,Y}$) for all stimuli pairs. The *outer axes* denote the stimulus values that elicited the responses (α_0 and α_1). The *inner axes* show $\gamma_{X,Y}$ for a particular stimuli pair as a function of time. The *y*-axis of the *inner plots* is the $\gamma_{X,Y}$ in multiples of 10^{-4} ($\gamma/10^{-4}$) and is dimensionless
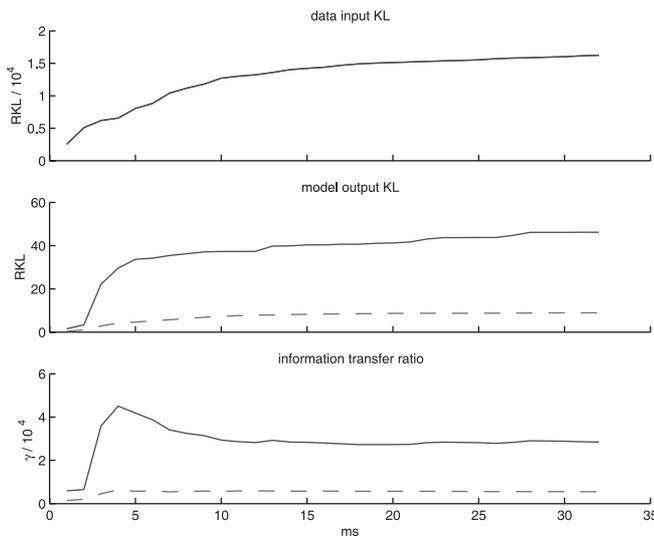
Fig. 10. Information processing characteristics of a simple time-varying system. The input processes are an example pair of EPSP responses from SF recordings. Their cumulative RKL distances are shown in the *top panel*. *The middle panel* shows the cumulative RKL for the simple theoretical spike generator output. The *bottom panel* shows the time-varying ratio of RKL distances ($\gamma_{X,Y}$) for the theoretical system. The *solid line* denotes results from the intensity function in (9), and the *dotted lines* represent results when $B = 0$

$\gamma_{X,Y}$ ranged between 10^{-4} and 10^{-3}, reaching the largest values during transient responses. These results depend on the specific stimulus condition used in the analysis. The present stimulus is biologically relevant and generates an information-bearing response in the SF. Additionally, the same analysis has been carried out using other stimulus features and the results were never higher than 10^{-2} (Rozell 2002). As described in Sect. 1.2, $0 \leq \gamma_{X,Y} \leq 1$, with a value of zero representing total

information loss about the stimulus change. The large decrease in information content we measured is counterintuitive as a system design, where we generally want to minimize unrecoverable loss in the early stages. As always, the accuracy of data analysis is limited by underlying assumptions and the amount of available data. The need for more data is evident in the size of the error bar lower bounds, but the order of magnitude of $\gamma_{X,Y}$ is clear. Our significant assumptions are the Gaussianity of the EPSP noise and independent bins in the spike response. We statistically verified the marginal normality of the EPSP noise in stationary segments and detailed the nonstationarities during EPSP activity. Using simulated data with the same first-order interbin dependencies as the SF data, we find that we underestimate the true spike RKL by a factor of two by assuming independent bins. This factor does not change the order of magnitude of our results.

It is imperative to remember that $\gamma_{X,Y}$ measures information present in the spike train output *relative* to information available in the EPSP input. Despite the low values measured for the SF information transfer efficiency for this stimulus, we know that the stimulus induces an information-bearing response in the SF and enough information is extracted from that response to mediate an eyestalk reflex. There may be enough information in the spike train output to make basic differentiations of the stimulus, but the present consideration is how well those decisions *could* be made by observing the EPSP inputs instead. In other words, how efficient is the SF voltage to impulse encoder at communicating the information contained in the EPSP? The results are striking and raise a significant question: Is the high-fidelity EPSP overdetermined for the information conveyed at the output, or are there stimulus conditions in which the output might better reflect the fidelity of the input signal? When investigating the theoretical analog

to point-process converter in Sect. 3.1, spike rates comparable to SF rates produced comparable information processing characteristics, and increasing the spike rate increased $\gamma_{X,Y}$ proportionally. Thus, spike rates limit the fidelity of voltage to impulse encoders. The stimuli used in this analysis produced discharge rates that are too low to convey the vast amount of stimulus information contained in the (high SNR) analog EPSPs. We conclude that the crayfish SF may be severely limited in its information processing capabilities by the low spike rates typically produced.

In another study (Juusola and French 1997), the "information efficiency" from EPSP to spike train in a spider slit-sense mechanoreceptor neuron was found to be ∼14%. There, efficiency is measured as a ratio of capacities from one stage to another. As stated in Sect. 1.2, analyses based on RKL distances and capacities are not comparable in general. Capacity cannot be directly related to information extraction performance metrics as can the KL distance. Therefore, even though our results differ by at least an order of magnitude, their results are not inconsistent with the analysis presented here. Indeed, the responses in Juusola and French (1997) appear to have SNRs and spike rates comparable to those of the crayfish SF, and if our analysis were carried out on their data, the results would be of the same order of magnitude as we calculated in the crayfish SF.

Plotting $\gamma_{X,Y}$ as a function of time revealed an interesting trend in the dynamic SF information processing capabilities. The encoding efficiency generally increases immediately after stimulus onset, followed by a slow decrease to steady-state values. The peak could be as much as an order of magnitude larger than the sustained value. Crayfish ocular reflexes to sudden-onset visual stimuli can be completed within about 400 ms after the transient spike response (Miller et al. 2002). Accounting for the latency in motor neurons and muscle contractions, the stimulus information conveyed in the reflex behavior must be communicated through the SF within 300 ms after stimulus onset. Reflex behavior therefore depends on the transient spike response, which corroborates the observed time-varying SF information processing characteristics. The amount of information being transmitted about a stimulus from input to output may have overall low values, but the SF is communicating the majority of that information during the transient response.

The SF information processing capabilities appear to be limited in part by the discharge rates present at the output, which clearly depend on the value of the input EPSP $(X(t))$. The performance increase during the transient response may be because of significant firing rate increases due to a dependence on *changes* in the EPSP $\left(\frac{\mathrm{d}X(t)}{\mathrm{d}t}\right)$. The same behavior was observed with the simple analog to point-process converter described in Sect. 3.1 when the outputs were explicitly dependent on recent changes in the input. The dynamic information processing characteristics are not evident when the output only depends on the current input value. With dependence only on the present input value $(X(t))$ and not on its derivative $\left(\frac{\mathrm{d}X(t)}{\mathrm{d}t}\right)$, the system would transfer information about stimulus changes with the same efficiency as it transfers information about sustained values. The transient nature of $\gamma_{X,Y}$ is consistent with a system meant to encode stimulus *changes* more efficiently than absolute stimulus values.

Appendix

Correlation structure of a nonstationary system

The membrane noise component of the SF EPSP is conceptualized as the output of the system shown in Fig. 3 responding to white noise input $w(k) \sim N\left(0, \sigma_w^2\right)$. The unit-sample response describing the time-varying membrane is given in (7) as

$$h(n,k) = \left(\prod_{l=k+1}^{n} a(l)u(n-k) \right) + \delta(n-k) \ .$$

The membrane noise can therefore be written explicitly as

$$
\begin{aligned}
(X(n) - \mu(n)) &= \sum_{k=-\infty}^{n} h(n,k)w(k) \\
&= w(n) \\
&\quad + \sum_{l=1}^{\infty} \left(\prod_{k=n-l+1}^{n} a(k)w(n-l) \right) ,
\end{aligned}
\qquad (10)
$$

where $X \sim N(\boldsymbol{\mu}, \mathbf{K})$. Substituting (10) into the definition of the covariance matrix, the expression for the element in the n-th row and m-th column reduces to

$$
\begin{aligned}
\mathbf{K}(n,m) &= \mathrm{E}[(X(n) - \mu(n))(X(m) - \mu(m))] \\
&= \sigma_w^2 \Bigg[\delta(m-n) \\
&\quad + \left(\prod_{k=m+1}^{n} a(k) \right) + \left(\prod_{r=n+1}^{m} a(r) \right) \\
&\quad + \sum_{l=1}^{\infty} \left(\prod_{k=n-l+1}^{n} a(k) \prod_{r=n-l+1}^{m} a(r) \right) \Bigg] \ .
\end{aligned}
$$

If the pole is stationary at a_0, then $\sigma^2 = \mathrm{E}[(X(n) - \mu(n))^2] = \sigma_w^2/(1 - a_0^2)$. We estimate σ_w^2 from measurements of σ^2 and a_0 in the resting membrane.

References

Berger T (1971) Rate distortion theory. Prentice-Hall, Upper Saddle River, NJ

Conover W (1980) Practical nonparametric statistics, 2nd edn. Wiley, New York

Cover T, Thomas J (1991) Elements of information theory. Wiley, New York

Gruner C (1998) Quantifying information coding limits in sensory systems. PhD thesis, Rice University, Houston, TX

Hall P (1992) The bootstrap and Edgeworth Expansion. Springer, Berlin Heidelberg New York

Johnson D, Gruner C, Glantz R (2000) Quantifying information transfer in spike generation. Neurocomputing 32–33: 1047–1054

Johnson D, Gruner C, Baggerly K, Seshagiri C (2001) Information-theoretic analysis of neural coding. J Comp Neurosci 10: 47–69

Juusola M, French AS (1997) The efficiency of sensory information coding by mechanoreceptor neurons. Neuron 18: 959–968

Kirk M, Waldrop B, Glantz R (1982) The crayfish sustaining fibers: I. Morphological representation of visual receptive fields in the second optic neuropil. J Comp Physiol 146: 175–179

Kirk M, Waldrop B, Glantz R (1983) The crayfish sustaining fibers: II. Responses to illumination, membrane properties and adaptation. J Comp Physiol 150: 419–425

Miller C, Johnson D, Schroeter J, Myint L, Glantz R (2002) Visual signals in an optomotor reflex: systems and information theoretic analysis. J Comp Neurosci 13: 5–21

Miller C, Johnson D, Schroeter J, Myint L, Glantz R (2003) Visual responses of crayfish ocular motoneurons: an information theoretical analysis. J Comp Neurosci 15: 247–269

Oppenheim A, Schafer R, Buck J (1999) Discrete-time signal processing, 2nd edn. Prentice-Hall, Upper Saddle River, NJ

Papoulis A (1965) Probability, random variables, and stochastic processes. McGraw-Hill, New York

Rozell C (2002) Analyzing dynamics and stimulus feature dependence in the information processing of crayfish sustaining fibers. Master's thesis, Rice University, Houston, TX

Shannon C, Weaver W (1949) The mathematical theory of communication. University of Illinois Press, Urbana, IL

Siebert W (1986) Circuits, signals, and systems. MIT Press, Cambridge, MA

Waldrop B, Glantz R (1985) Synaptic mechanisms of a tonic EPSP in crustacean visual interneurons: analysis and simulation. J Neurophysiol 54(3): 636–650

Wiersma C, Yamaguchi T (1966) The neuronal components of the optic nerve of the crayfish as studied by single unit analysis. J Comp Neurol 138: 337–358